Eur. Phys. J. C (2026) 86:286
https://doi.org/10.1140/epjc/s10052-026-15505-6

THE EUROPEAN PHYSICAL JOURNAL C

Regular Article - Theoretical Physics

Probing strong-gravity chaos and stability of circular photon orbits around the Kerr–Sen black hole

Pradeep Singh[1,a], **Hemwati Nandan**[2,b], **Shubham Kala**[3,c], **Nidhi Handa**[4,d], **Lokesh Kumar Joshi**[1,e], **G. Mustafa**[5,6,f]

[1] Department of Applied Sciences, Faculty of Engineering and Technology, Gurukula Kangri (Deemed to be University), Haridwar 249404, India
[2] Department of Physics, Hemwati Nandan Bahuguna Garhwal University, Srinagar, Uttarakhand 246174, India
[3] The Institute of Mathematical Sciences, C.I.T. Campus, Taramani, Tamil Nadu 600113, India
[4] Department of Mathematics and Statistics, Gurukula Kangri (Deemed to be University), Haridwar 249404, India
[5] Department of Physics, Zhejiang Normal University, Jinhua 321004, China
[6] Research Center of Astrophysics and Cosmology, Khazar University, 41 Mehseti Street, AZ1096 Baku, Azerbaijan

Received: 3 February 2026 / Accepted: 26 February 2026

Abstract This study presents a detailed investigation of the dynamics of massless test particles (photons) to analyze the stability of null circular geodesics around the Kerr–Sen black hole (KSBH) spacetime. KSBH is a new solution arising in the low-energy effective field theory of heterotic string theory. The analysis proceeds by obtaining the radial effective potential, which serves as the foundation for calculating the Lyapunov exponent, a central quantity used to describe the stability or instability of geodesic motion in dynamical systems. The study employs the Lyapunov exponent approach to determine the stability or instability of circular orbits under varying values of the charge parameter Q and Kerr parameter a. Additionally, the analytical expressions for the radius of circular photon orbits and the corresponding impact parameter, defined as the ratio of conserved angular momentum to energy are also derived explicitly. To further analyze the orbital behavior, techniques such as Poincaré maps, the Lyapunov Exponent, and FLI are utilized to distinguish between regular and chaotic trajectories. The sign and magnitude of the Lyapunov exponent provide a rigorous criterion to distinguish between stable and unstable circular orbits. These results contribute to a deeper understanding of the geodesic structure and perturbative stability in string-inspired rotating charged black hole backgrounds. The findings are also compared with those of the KBH case to highlight the impact of the BH charge on the stability of null geodesics. This study provides deeper insights into the dynamical properties of null geodesics in charged rotating BH spacetimes in GR and alternative theory of gravity.

1 Introduction

The string theory is known as one of the most popular candidate theories to unify all four fundamental forces in nature [1]. Like the classical theory of gravity i.e. GR, string theory also admits the BH solutions in general [2,3]. In GR, the first-ever rotating BH solution was mathematically described by Kerr in 1963 [4,5]. A few years later, Sen employed a certain solution-generating technique on the KBH solution to derive the metric for charge rotating BH solution in low energy limit of the heterotic string theory and the obtained solution thus named as Kerr–Sen BH (KSBH) [6–9]. The KSBH solution is different from the KBH solution as it is characterized by three parameters (mass, angular momentum and charge) and arose from heterotic string theory while the KBH solution is parameterized by only two parameters (mass and angular momentum) which was formulated in GR [10–12].

The geodesics structure of massive and massless particles in the equatorial plane of the various spacetime backgrounds have been extensively studied to understand the gravity around the BH [13,14]. The stability of geodesics plays an important role in explaining the nature of the trajectories of particles around the BH. Basically, the geodesics in KSBH spacetime are nonlinear differential equations, there-

[a] e-mail: pradeep.dawan@gmail.com
[b] e-mail: hnandan@associates.iucaa.in
[c] e-mail: shubhamkala871@gmail.com
[d] e-mail: handanidhi1@gmail.com
[e] e-mail: lokesh.joshe@gmail.com
[f] e-mail: gmustafa3828@gmail.com (corresponding author)

Published online: 18 March 2026

fore, we use here the Lyapunov exponent criteria to investigate the stability of geodesics [15–20].

The Lyapunov exponent measures the average rate of separation between nearby trajectories in any classical phase space and may have positive, negative or zero value [21–25]. The radial effective potential obtained from the geodesics equation is a basic approach to understand the orbits of test particles around any BH spacetime. Therefore, in order to analyze the stability of geodesics, the Lyapunov exponent is widely used whose formulation in terms of radial effective potential is derived and discussed in Sect. 2 in detail [26,27]. The real value of the Lyapunov exponent indicates unstable circular geodesics, the imaginary value of the Lyapunov exponent indicates stable circular geodesics and the vanishing Lyapunov exponent implies marginally stable geodesics [28].

The stability analysis of geodesics in the equatorial plane around the various interesting BH spacetime geometry has already been investigated by several authors [21,26,29–39]. The stability of geodesics and quasinormal modes of a dual stringy BH, (2+1) dimensional charged BTZ BH spacetime and non-commutative Schwarzschild BH (NCSBH) via Lyapunov exponent are also examined in detail [29,40,41]. The stability of circular geodesics around the RNBH, KNBH and charged Myres–Perry BH spacetimes have been studied via calculating the Lyapunov exponent (proper time and coordinate time Lyapunov exponent) [26,27,42].

Lyapunov-based chaos indicators provide powerful tools for characterizing the stability and chaotic nature of photon trajectories in curved spacetimes [43]. In particular, the Largest Lyapunov Exponent (LLE) quantifies the average exponential rate at which nearby trajectories in phase space diverge, thereby serving as a direct measure of orbital instability and sensitivity to initial conditions [44]. A positive value of the LLE indicates chaotic motion, while a vanishing or negative value corresponds to regular dynamics. Complementarily, the fast Lyapunov indicator (FLI) offers an efficient numerical diagnostic to distinguish between regular and chaotic orbits over relatively short integration times by monitoring the rapid growth of deviation vectors [45]. These indicators have been widely employed in studies of dynamical systems and BH spacetimes and are especially suitable for investigating the stability of circular photon orbits [46–50]. In the present work, we use both the LLE and FLI to systematically analyze the onset of chaos and the stability properties of photon motion around the KSBH, thereby providing a physically transparent and robust characterization of strong-gravity chaos in this spacetime. The main objective of this work is to compute the Lyapunov exponent explicitly to investigate the stability of the null circular geodesics in the equatorial plane for KSBH spacetime. Furthermore, to analyze the more complex behavior (regular or chaotic orbit) of the KSBH, Poincare map and FLI are also investigated for the null case. The present paper is organized as follows: In Sect. 2, we briefly review the basic concepts of the Lyapunov exponent and the expression of the Lyapunov exponent in terms of the radial effective potential. In Sect. 3, a brief introduction of KSBH spacetime is presented and the expression of the radial effective potential for the given spacetime is derived. In Sect. 4, we explicitly derived the Lyapunov exponent for the null circular geodesics and investigated its stability aspects. To further examine the orbital behavior, techniques such as Poincaré maps, the Lyapunov Exponent, and FLI are utilized to distinguish between regular and chaotic trajectories. Finally, in Sect. 5, we have summarised our results.

2 Lyapunov exponent in terms of Radial effective potential

In classical phase space, the Lyapunov exponent of a dynamical system is the quantity that measures the rate of convergence and divergence between two nearby trajectories (geodesics) [24].
Mathematically, two trajectories in any phase space with initial separation vector $\delta Z(0)$ diverge at a rate given by

$$|\delta Z(t)| = e^{\lambda t}|\delta Z(0)|. \tag{1}$$

The expression for the Lyapunov exponent comes out as,

$$\lambda = \frac{1}{t} ln \frac{|\delta Z(t)|}{|\delta Z(0)|}. \tag{2}$$

Here, λ denotes the Lyapunov exponent, t is the evolution time, $\delta Z(t)$ represents the deviation (separation) vector between two neighboring trajectories in phase space, and $|\delta Z(0)|$ is the magnitude of the initial separation vector. The Lyapunov exponent can be positive, negative, or zero. A positive value of λ indicates exponential divergence of nearby geodesics and hence chaotic behavior, whereas a negative value corresponds to convergence, and $\lambda = 0$ characterizes marginally stable or regular motion [51,52].

To derive the expression of Lyapunov exponent in terms of the radial effective potential, we consider the general stationary axi-symmetric spacetime geometry [21,26,27],

$$dS^2 = g_{tt}dt^2 + 2g_{t\phi}dtd\phi + g_{rr}dr^2 + g_{\theta\theta}d\theta^2 + g_{\phi\phi}d\phi^2. \tag{3}$$

The Lagrangian for a test particle in the equatorial plane around this spacetime is given as

$$\mathcal{L} = \frac{1}{2}[g_{tt}\dot{t}^2 + 2g_{t\phi}\dot{t}\dot{\phi} + g_{rr}\dot{r}^2 + g_{\phi\phi}d\dot{\phi}^2]. \tag{4}$$

The conjugate momenta for r coordinate is then derived as,

$$p_r = \frac{\delta\mathcal{L}}{\delta\dot{r}} = \dot{r}g_{rr}, \tag{5}$$

and by applying Euler–Lagrange's equation of motion for r coordinate, we get,

$$\frac{dp_r}{dt} = \frac{\delta \mathcal{L}}{\delta r}. \tag{6}$$

Using Eqs. (5) and (6), the system of nonlinear differential equation in two-dimensional phase space with variable (p_r, r) is obtained as,

$$\begin{cases} \dot{p}_r = \frac{\delta \mathcal{L}}{\delta r}, \\ \dot{r} = \frac{p_r}{g_{rr}}. \end{cases} \tag{7}$$

Now by applying the linearization process to the above system of differential equations, the evolution matrix is derived as [51],

$$M_{ij} = \begin{bmatrix} 0 & \frac{d}{dr}\dot{p}_r \\ \frac{1}{g_{rr}} & 0 \end{bmatrix}. \tag{8}$$

The eigenvalues of this matrix provide information about the stability of circular geodesics and are well known as principal Lyapunov exponent which is obtained as,

$$\lambda^2 = \frac{1}{g_{rr}} \frac{d}{dr}\left(\frac{\delta \mathcal{L}}{\delta r}\right). \tag{9}$$

Now, after some simplification, Lagrange's equation of motion, $\frac{d}{dT}\left(\frac{\delta \mathcal{L}}{\delta \dot{r}}\right) - \frac{\delta \mathcal{L}}{\delta r} = 0$ reduced as,

$$\frac{\delta \mathcal{L}}{\delta r} = \frac{1}{2g_{rr}} \frac{d}{dr}\left(\dot{r} g_{rr}\right)^2. \tag{10}$$

Thus by using the above equation the principal Lyapunov exponent obtained in Eq. (9) can be rewritten as,

$$\lambda^2 = \frac{1}{2g_{rr}} \frac{d}{dr}\left[\frac{1}{g_{rr}} \frac{d}{dr}(\dot{r} g_{rr})^2\right]. \tag{11}$$

Further simplifying the above Eq. (11) and using the condition of circular orbits i.e. $\dot{r}^2 = 0, (\dot{r}^2)' = 0$, the principal Lyapunov exponent reduces to [52],

$$\lambda = \sqrt{\frac{(\dot{r}^2)''}{2}}. \tag{12}$$

From Eq. (12), one can observe that, for the unstable circular geodesics, λ should be real i.e. $(\dot{r}^2)'' > 0$, for the stable circular geodesics, λ should be imaginary i.e. $(\dot{r}^2)'' < 0$ and the circular geodesics are marginally stable when Lyapunov exponent vanishes i.e. $(\dot{r}^2)'' = 0$.

3 Geodesics around Kerr–Sen black hole spacetime

The rotating charged black hole arising from heterotic string theory was obtained by Sen using a solution-generating technique applied to the Kerr black hole solution and is commonly known as the KSBH spacetime [11,53–57]. In Boyer-Lindquist coordinates, the line element of KSBH spacetime reads as

$$\begin{aligned} dS^2 = &-\left(\frac{\Delta - a^2 \sin^2\theta}{\rho^2}\right) dt^2 - \left(\frac{4Mra \sin^2\theta}{\rho^2}\right) d\phi dt \\ &+ \frac{\rho^2}{\Delta} dr^2 + \rho^2 d\theta^2 + \Big(\rho^2 + a^2 \sin^2\theta \\ &+ \frac{2Mra^2 \sin^2\theta}{\rho^2}\Big) \sin^2\theta d\phi^2, \end{aligned} \tag{13}$$

where, $\rho^2 = r(r+q) + a^2 \cos^2\theta$ and $\Delta = r(r+q) - 2Mr + a^2$. Here, q stands for $\frac{Q^2}{M}$; where, Q and M represent the charge and mass of the BH, respectively, and $a = J/M$ represent the specific angular momentum of the BH with angular momentum (J).

To analyze the stability of circular geodesics in the equatorial plane (i.e. $\theta = \pi/2$) of KSBH spacetime the geometry of KSBH spacetime is reduced as

$$\begin{aligned} dS^2 = &-\left(1 - \frac{2M}{r+q}\right) dt^2 - \left(\frac{4Ma}{r+q}\right) dt d\phi + \frac{r(r+q)}{\Delta} dr^2 \\ &+ \left(r(r+q) + a^2 + \frac{2Ma^2}{r+q}\right) d\phi^2, \end{aligned} \tag{14}$$

where, $\Delta = r(r+q) - 2Mr + a^2$. To describe the geodesics motion around KSBH spacetime, the Lagrangian can be written as,

$$\begin{aligned} 2\mathcal{L} = &-\left(1 - \frac{2M}{r+q}\right) \dot{t}^2 - \left(\frac{4Ma}{r+q}\right) \dot{t}\dot{\phi} + \frac{r(r+q)}{\Delta} \dot{r}^2 \\ &+ \left(r(r+q) + a^2 + \frac{2Ma^2}{r+q}\right) \dot{\phi}^2. \end{aligned} \tag{15}$$

Here, dot (.) represents the differentiation with respect to affine parameter τ.

The generalized momenta from the Lagrangian can be obtained as,

$$p_t = -\left(1 - \frac{2M}{r+q}\right) \dot{t} - \left(\frac{2Ma}{r+q}\right) \dot{\phi} = -E, \tag{16}$$

$$p_\phi = -\left(\frac{2Ma}{r+q}\right) \dot{t} + \left(r(r+q) + a^2 + \frac{2Ma^2}{r+q}\right) \dot{\phi} = L, \tag{17}$$

$$p_r = \frac{r(r+q)}{\Delta} \dot{\phi}. \tag{18}$$

where, E and L are the energy and angular momentum of the particle moving around the KSBH respectively. Since the Lagrangian does not depend on 't' and 'ϕ', so the quantities p_t and p_ϕ are conserved. Now by solving the Eqs. (16) and (17), the first integral of the geodesics for time and phase component of the four-momentum of the particle with a constant of motion E and L are obtained as,

$$\dot{t} = \frac{1}{\Delta}\left[\left(r\,(r+q) + a^2 + \frac{2Ma^2}{r+q}\right)E - \left(\frac{2Ma}{r+q}\right)L\right], \tag{19}$$

$$\dot{\phi} = \frac{1}{\Delta}\left[\left(1 - \frac{2M}{r+q}\right)L + \left(\frac{2Ma}{r+q}\right)E\right]. \tag{20}$$

The Hamiltonian for the motion of particles around the spacetime is derived as,

$$2H = -\left(1 - \frac{2M}{r+q}\right)\dot{t}^2 - \left(\frac{4Ma}{r+q}\right)\dot{t}\dot{\phi} + \frac{r\,(r+q)}{\Delta}\dot{r}^2 + \left(r\,(r+q) + a^2 + \frac{2Ma^2}{r+q}\right)\dot{\phi}^2 = K, \tag{21}$$

where, $K = 0$ and $K = -1$ correspond to null and timelike geodesics respectively.

After substituting the value of $\dot{t}$ and $\dot{\phi}$ from Eqs. (19) and (20) in the Eq.(21), the radial equation of motion for charged rotating KSBH spacetime is obtained as,

$$\dot{r}^2 = E^2 + K - \frac{2KM}{r+q} - \frac{L^2 - a^2\left(E^2 + K\right)}{r\,(r+q)} + \frac{2M\,(L - aE)^2}{r\,(r+q)^2}. \tag{22}$$

By substituting the values of K in Eq. (22), one can obtain the radial equation for timelike as well as null geodesics and also can derive the effective potentials for both cases of geodesics.

4 Qualitative analysis

In this section, the qualitative investigation of Lyapunov stability is carried out by computing the Lyapunov exponent for the null geodesics around the KSBH spacetime. Poincare map, Lyapunov exponent and FLI are also analyzed for the null circular geodesics.

4.1 Null circular geodesics

In the context of GR, null circular orbits describe the motion of massless particles (photons) that maintain circular trajectories around a gravitational source. These orbits play a critical role in BH studies, as they are fundamentally linked to observable phenomena like BH shadows, gravitational lensing, and the overall dynamical structure of spacetime.

By substituting $K = 0$ in Eq. (22) the radial equation corresponding to null geodesics is reduced as,

$$\dot{r}^2 = E^2 - \frac{L^2 - a^2E^2}{r(r+q)} + \frac{2M\,(L - aE)^2}{r(r+q)^2}. \tag{23}$$

The first derivative of above equation with respect to r is given as,

$$(\dot{r}^2)' = \frac{(L^2 - a^2E^2)(2r+q)}{r^2(r+q)^2} - \frac{2M\,(L - aE)^2\,(3r+q)}{r^2(r+q)^3}. \tag{24}$$

For the null circular geodesics, we equate $\dot{r}^2 = 0$ and $(\dot{r}^2)' = 0$ and obtained two equations as,

$$E_c^2 - \frac{L_c^2 - a^2E_c^2}{r_c(r_c+q)} + \frac{2M(L_c - aE_c)^2}{r_c(r_c+q)^2} = 0, \tag{25}$$

and

$$\frac{(L_c^2 - a^2E_c^2)(2r_c+q)}{r_c^2(r_c+q)^2} - \frac{2M(L_c - aE_c)^2(3r_c+q)}{r_c^2(r_c+q)^3} = 0. \tag{26}$$

Now, let us take $L_c - aE_c = x$ which provides $L_c^2 - a^2E_c^2 = x^2 + 2axE_c$. By substituting these two quantities into the above equations and reduce to,

$$E_c^2 = \frac{x^2 + 2axE_c}{r_c(r_c+q)} - \frac{2Mx^2}{r_c(r_c+q)^2}, \tag{27}$$

and

$$\frac{(x^2 + 2axE_c)(2r_c+q)}{r_c^2(r_c+q)^2} - \frac{2Mx^2(3r_c+q)}{r_c^2(r_c+q)^3} = 0. \tag{28}$$

From the Eq. (28), we can obtain,

$$x^2 + 2axE_c = \frac{2Mx^2(3r_c+q)}{(r_c+q)(2r_c+q)}. \tag{29}$$

Now substituting the value of $x^2 + 2axE$ from Eq. (29) in the Eq. (27) we get,

$$E_c^2 = \frac{2Mx^2}{(r_c+q)^2(2r_c+q)}. \tag{30}$$

Then by eliminating E from the Eqs. (29) and (30), we have obtained an equation follows as,

$$(r_c+q)^2(2r_c+q)^2-4M(r_c+q)(2r_c+q)(3r_c+q)+4M^2(3r_c+q)^2-8Ma^2(2r_c+q)=0 \quad (31)$$

From the above equation, one can calculate the radius of null circular orbits around KSBH spacetime.

Further simplifying Eq. (30), one can obtain the expression for the impact parameter $D_c=\frac{L_c}{E_c}$ as,

$$D_c=\frac{L_c}{E_c}=a+(r_c+q)\sqrt{\frac{2r_c+q}{2M}}. \quad (32)$$

4.2 Lyapunov exponent

The Lyapunov exponent offers a precise and quantitative framework for analyzing the stability of geodesic motion in KSBH spacetimes. By evaluating the second derivative of the effective potential, one can determine the dynamical nature of orbits and identify transitions between stable, unstable, and chaotic behavior. The second derivative of radial effective potential is obtained as,

$$(\dot{r}^2)''=-\frac{2(L^2-a^2E^2)(3r^2+3rq+q^2)}{r^3(r+q)^3}+\frac{4M\left(L-aE\right)^2\left(6r^2+4rq+q^2\right)}{r^3(r+q)^4}. \quad (33)$$

Now by using the formula $\lambda=\sqrt{\frac{(\dot{r}^2)''}{2}}$, we have explicitly derived the Lyapunov exponent for the null circular geodesics as,

$$\lambda_{null}=\sqrt{\frac{2M\left(L_c-aE_c\right)^2\left(6r_c^2+4r_cq+q^2\right)}{r_c^3(r_c+q)^4}-\lambda_1}. \quad (34)$$

where

$$\lambda_1=\frac{(L_c^2-a^2E_c^2)(3r_c^2+3r_cq+q^2)}{r_c^3(r_c+q)^3}.$$

For the stable circular orbits, the Lyapunov exponent λ_{null} should be imaginary for which

$$\frac{2M\left(L_c-aE_c\right)^2\left(6r_c^2+4r_cq+q^2\right)}{r_c^3\left(r_c+q\right)^4}<\frac{(L_c^2-a^2E_c^2)\left(3r_c^2+3r_cq+q^2\right)}{r_c^3\left(r_c+q\right)^3}. \quad (35)$$

After further simplification of the above inequality, the condition for the stable circular orbits is obtained as,

$$\frac{L_c}{E_c}<\frac{\left[2M\left(6r_c^2+4r_cq+q^2\right)+(r_c+q)\left(3r_c^2+3r_cq+q^2\right)\right]a}{2M\left(6r_c^2+4r_cq+(q)^2\right)-(r_c+q)\left(3r_c^2+3r_cq+q^2\right)} \quad (36)$$

Similarly, for the unstable circular orbits, λ_{null} should be real, for which

$$\frac{2M\left(L_c-aE_c\right)^2\left(6r_c^2+4r_cq+q^2\right)}{r_c^3\left(r_c+q\right)^4}>\frac{(L_c^2-a^2E_c^2)\left(3r_c^2+3r_cq+q^2\right)}{r_c^3\left(r_c+q\right)^3}. \quad (37)$$

The above inequality can be simplified as below,

$$\frac{L_c}{E_c}>\frac{\left[2M\left(6r_c^2+4r_cq+q^2\right)+(r_c+q)\left(3r_c^2+3r_cq+q^2\right)\right]a}{2M\left(6r_c^2+4r_cq+(q)^2\right)-(r_c+q)\left(3r_c^2+3r_cq+q^2\right)} \quad (38)$$

Therefore, the stable null circular orbits are found for when $\frac{L_c}{E_c}<\frac{(2MY+X)a}{2MY-X}$, while the unstable null circular orbits are found when $\frac{L_c}{E_c}>\frac{(2MY+X)a}{2MY-X}$, where, $X=(r_c+q)\left(3r_c^2+3r_cq+(q)^2\right)$ and $Y=\left(6r_c^2+4r_cq+(q)^2\right)$.

4.3 Poincaré section and Lyapunov indicator

The Poincaré section and FLI are powerful and complementary diagnostic tools in the analysis of nonlinear dynamical systems, especially in the study of orbital stability in BH spacetimes. These methods are particularly effective in revealing complex dynamical behavior that may not be easily discernible through direct integration of geodesic equations alone. In the context of GR, where the phase space can become highly intricate due to the curvature and rotation of spacetime, such tools are indispensable. The Poincaré section reduces a continuous-time dynamical system to a discrete map by recording the successive intersections of a particle's trajectory with a predefined hypersurface transverse to the flow. On the other hand, FLI offers a highly sensitive and computationally efficient means of quantifying dynamical stability. Unlike classical Lyapunov exponents, which require long integration times to converge, the FLI measures the exponential divergence of nearby trajectories over shorter timescales.

In BH dynamics, such as those described by Kerr or Kerr–Sen geometries, the Poincaré section plays a vital role in analyzing how orbits evolve near critical regions like the ISCO or within the ergosphere, where gravitational and rotational effects are most intense. In our study of the KSBH spacetime,

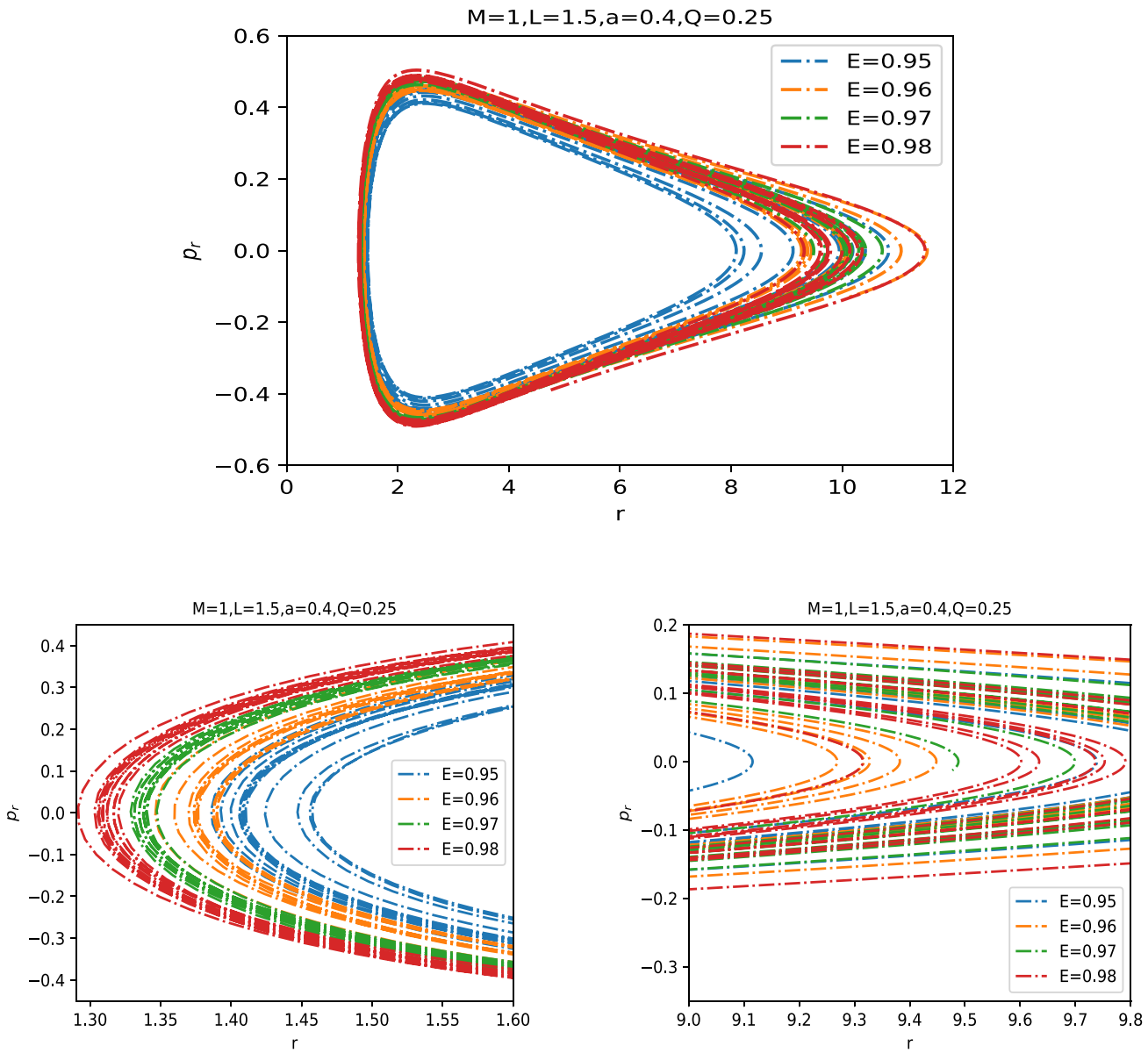

Fig. 1 Poincaré map of null geodesics in the KSBH for different energy levels, with the angular coordinate fixed at $\theta = \pi/2$ and $p_\theta > 0$. The upper panel shows the full phase-space structure, while the lower-left panel magnifies the leftmost island of the upper panel and the lower-right panel magnifies the rightmost island. These islands represent distinct regions of phase space in which the trajectories remain confined. The fixed parameter values used in each case are indicated at the top of the figure

the system's behavior is analyzed by using the Poincare section, Lyapunov exponent and FLI to investigate the chaotic dynamics of geodesics (Fig. 1).

From left to right in the upper panel of Fig. 2, increasing values of the spin and charge parameters lead to noticeable changes in the structure of the Poincaré maps. The lower panel of Fig. 2 compares the phase-space behavior of the KBH, the RNBH, and the KSBH. The KBH exhibits predominantly regular motion characterized by well-defined islands of stability and periodic orbits, while the RNBH shows comparatively simpler dynamics with trajectories confined to fewer regions of phase space. In contrast, the KSBH displays significantly more intricate and complex structures due to the combined influence of both spin and charge, indicating enhanced chaotic behavior. This comparison demonstrates that while all three spacetimes share common features of photon orbital dynamics, the inclusion of charge and rotation in the KSBH introduces richer dynamical patterns and stronger instability, emphasizing the important role of additional physical parameters in shaping the stability and

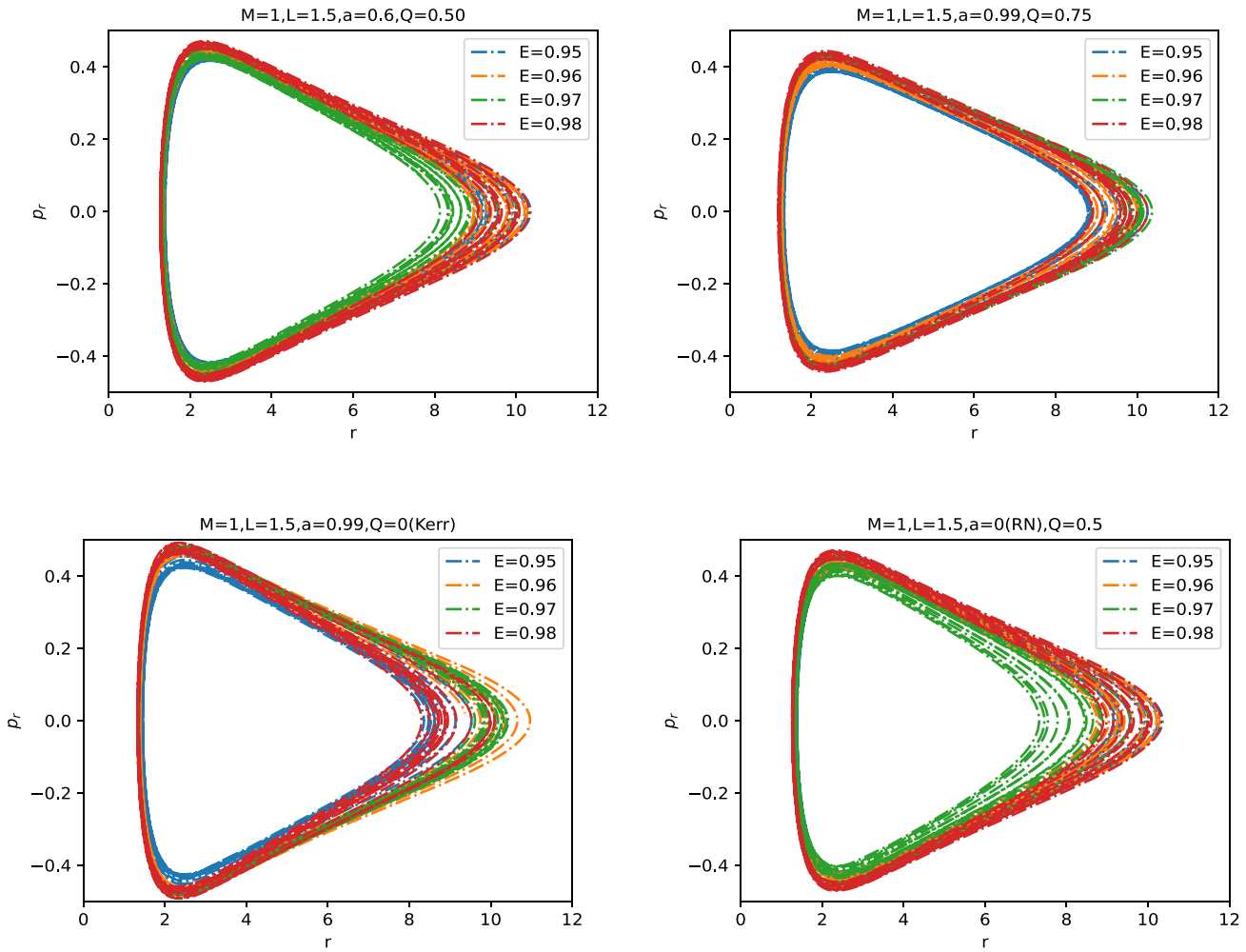

Fig. 2 Poincaré map of geodesics in the KSBH spacetime for different energy levels, with $\theta = \pi/2$ and $p_\theta > 0$, for various combinations of the spin and charge parameters. The upper-left panel corresponds to the low-charge, low-spin case, while the upper-right panel represents the high-charge, high-spin case. The lower-left panel shows the Kerr limit ($Q = 0$), and the lower-right panel corresponds to the Reissner–Nordström black hole ($a = 0$). The fixed parameter values used in each case are indicated at the top of the figure

chaotic nature of geodesic motion. The Poincaré sections were constructed by numerically integrating the equations of motion using an adaptive Runge–Kutta scheme implemented in the `solve_ivp` routine. The integration was performed over the interval $t \in [0, 5000]$ with a maximum step size $\Delta t_{\max} = 0.5$, and high numerical accuracy was ensured by adopting $\texttt{rtol} = \texttt{atol} = 10^{-9}$. The surface of section was defined by the condition $\phi = \pi/2$, and crossings with positive direction were recorded. Initial transient points were discarded to obtain reliable Poincaré maps. Using the proper time τ and a proper distance $d(\tau)$ between two nearby orbits to define the largest Lyapunov exponent as follows [48],

$$\lambda = \lim_{\tau\to\infty} \frac{1}{\tau} \ln \frac{d(\tau)}{d(0)}, \tag{39}$$

where $d(0)$ represents the initial separation between two nearby orbits. Such a definition is independent of a choice of spacetime coordinates. In the KSBH spacetime, the geometry is more complex due to additional coupling between gravitational, electromagnetic, and scalar fields. This richer structure gives rise to more intricate geodesic behavior, making stability analysis both challenging and essential. To assess the stability of a null circular geodesic, one can linearize the radial geodesic equation around a reference orbit r_0 and analyze the evolution of a small perturbation δr.

The variation of the Lyapunov exponents for different values of r_0 is depicted in Fig. 3. It is observed that the system is non-chaotic when the initial separation of orbits is small. Furthermore, the lowest value of r_0 is identified that leads to chaos, and as r_0 increases, the system transitions to a non-chaotic state. Additionally, as the values of the spin and charge parameters increase, the chaotic behavior of the system intensifies. This demonstrates that the spin and charge parameters enhance the chaotic behavior, causing the tra-

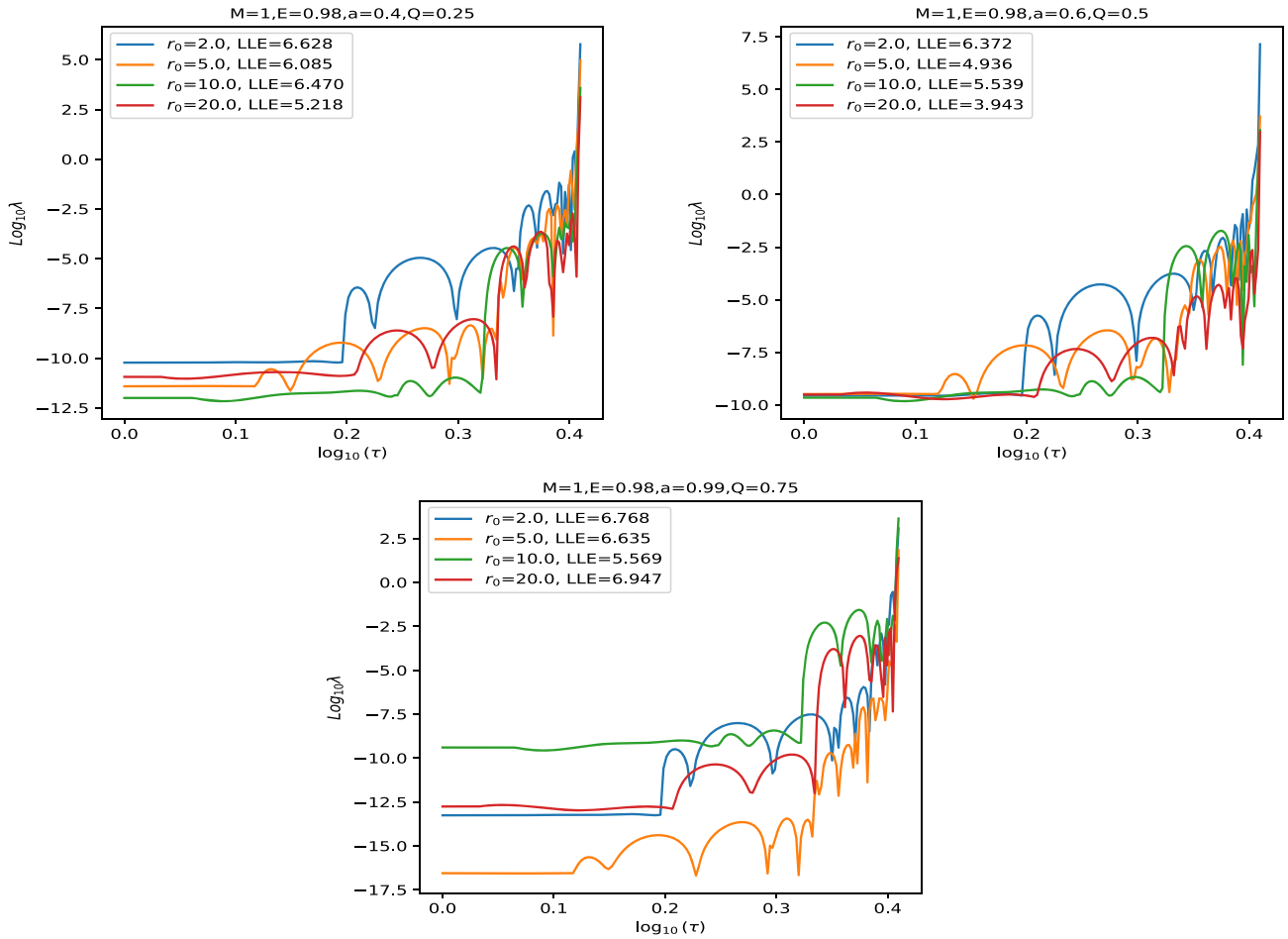

Fig. 3 Variation of Lyapunov exponents of the orbits for different values of r_0 with $\theta = \pi/2$ and $p_\theta > 0$. The fixed parameter values used in each case are indicated at the top of the figure

jectories to diverge exponentially over time. Out of all three cases it is graphically depicted that the largest observed value of the Lyapunov exponent is 7.017, which corresponds to the lowest value of $r_0 = 2$.

Indeed, the Lyapunov exponent measures chaos much clearer in view of both qualitative and quantitative aspects but it is also observed that obtaining the desired stable value of the Lyapunov exponent requires a longer time. In comparison, the FLI is a more sensitive tool for distinguishing chaos from order. Therefore, the FLI can be defined as follow [49],

$$FLI = \log_{10} \frac{d(\tau)}{d(0)}. \tag{40}$$

where, $d(0)$ is initial separation between two nearby trajectories or orbits and $d(\tau)$ is the separation between two nearby trajectories after proper time τ. In the context of GR, particularly those involving BH spacetimes, the FLI serves as an effective tool for analyzing the stability of geodesic motion. It is especially valuable when examining perturbed trajectories, motion confined to the equatorial plane, or the effects of additional fields such as scalar, electromagnetic, or dilaton fields. Unlike conventional methods based on effective potentials, the FLI provides a broader and more sensitive approach for probing orbital dynamics, making it particularly adept at revealing subtle instabilities and the onset of chaotic behavior in complex spacetime geometries. The FLI quantifies the divergence of nearby trajectories in phase space over time. In contrast to the maximal Lyapunov exponent (MLE), which involves computing the time-averaged growth rate, the FLI looks at the instantaneous growth of deviation vectors and is thus much faster and more sensitive for detecting chaos. The motion of the particle will be regular, if FLI grows linearly or slowly with time, while, the motion will be chaotic, if FLI grows exponentially or rapidly with time. The FLI, due to its time-resolved and non-averaged nature, is particularly effective at detecting local instabilities, intermittent chaos, and transitions between regular and chaotic behavior. It is especially useful in systems with mixed-phase space structures,

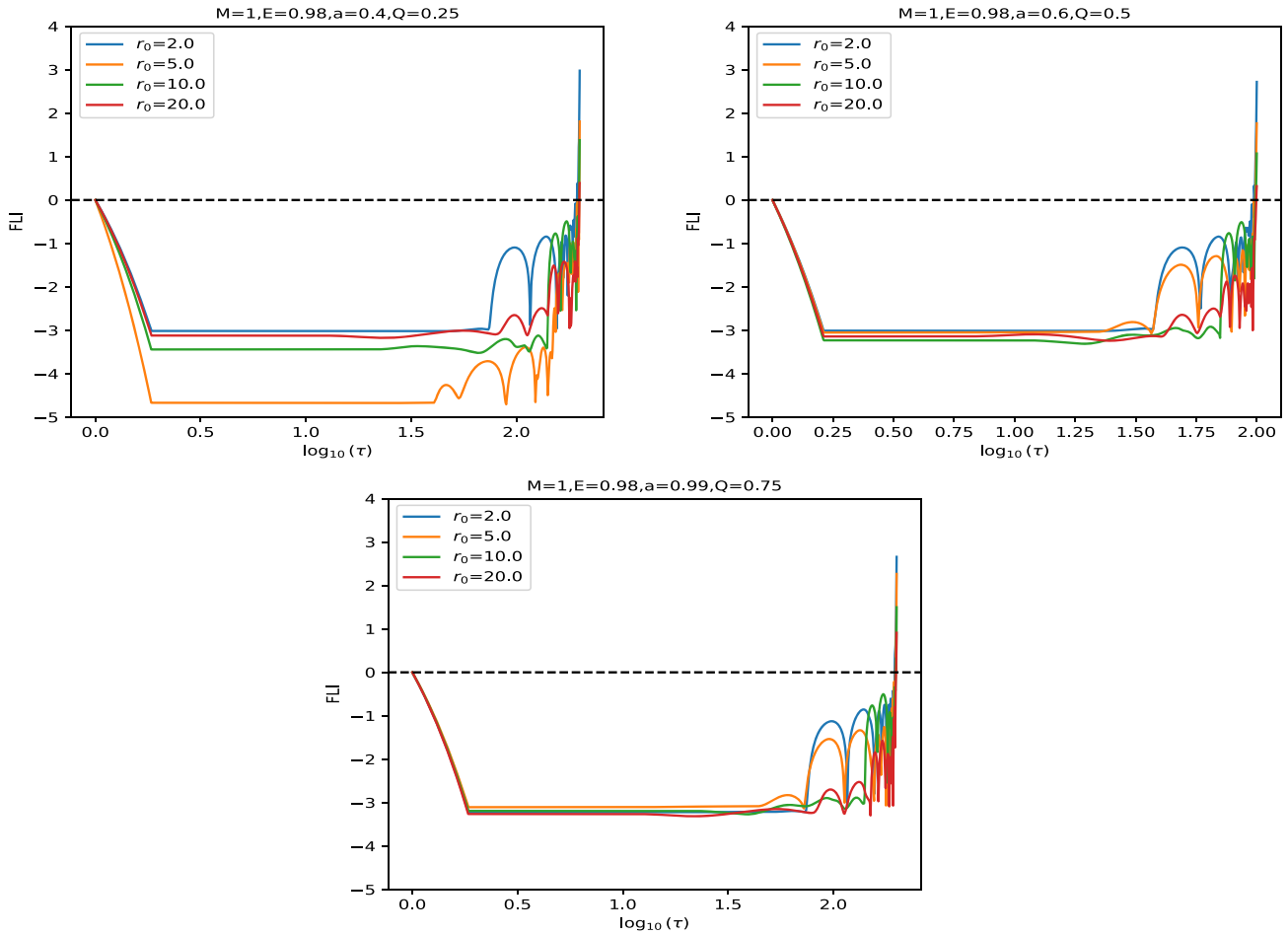

Fig. 4 Variation in FLI of the orbits for different values of r_0 with $\theta = \pi/2$ and $p_\theta > 0$. The fixed parameter values used in each case are indicated at the top of the figure

such as those found near the ISCO or within the ergosphere of rotating BHs.

In Fig. 4, the FLI represents the orbital chaotic behavior of the orbits. One can observe that non-chaotic, chaotic, and threshold behaviors depending on the initial separation of the orbits. Beyond a specific value of the initial separation, the FLI increases rapidly, indicating the chaotic behavior of the orbits. The FLI is maximum for the smallest value of r_0. However, for larger values of the spin and charge parameters, r_0 does not affect the FLI symmetrically. This suggests that the presence of the charge and spin parameters enhances the chaotic behavior of the orbits.

5 Conclusions

In this work, we analyzed the motion of massless particles in the Kerr–Sen black hole (KSBH) spacetime to investigate the stability of null circular geodesics on the equatorial plane. The results show that the combined presence of spin and charge significantly modifies the dynamical structure of photon orbits. The main results are summarized below

1. The study demonstrate that radial equation play key role to compute Lyapunov exponent which is and important tool to analyze the stability of circular orbits. Real Lyapunov exponent is correspond to the unstable circular orbits are while the imaginary value of Lyapunov exponent indicates the stable circular orbit.
2. We find that the properties of the photon sphere and the associated impact parameter are strongly influenced by the BH mass, spin, and charge. In particular, the inclusion of charge and rotation leads to appreciable deviations from the Kerr and Reissner–Nordström limits, highlighting the impact of string-inspired corrections in the KSBH geometry.
3. The nonlinear and chaotic behavior of geodesic motion was explored using Poincaré sections, the largest Lyapunov exponent, and the fast Lyapunov indicator (FLI). The Poincaré maps reveal the coexistence of regular and

chaotic regions in phase space, with well-defined islands corresponding to confined motion. The largest Lyapunov exponent signals the onset of chaos for specific initial conditions, while the FLI provides a more sensitive measure, detecting chaotic behavior at earlier stages of evolution.

4. The results clearly demonstrate that both spin and charge play a crucial role in enhancing the chaotic dynamics of null geodesics in the KSBH spacetime. In comparison with the KBH and RNBH, the KSBH exhibits a richer and more intricate phase-space structure, characterized by a greater diversity of unstable periodic orbits and extended chaotic regions. This increased complexity highlights the strong influence of additional physical parameters on photon motion and underscores the importance of considering charged and rotating BHs geometries when exploring nonlinear dynamics and chaos in strong gravitational fields.
5. The chaotic behavior of photon motion around the charged and rotating KSBH may have important astrophysical and observational implications. The combined effects of charge and rotation can modify photon trajectories, leading to measurable changes in BHs shadows and gravitational lensing patterns, as well as in the brightness distribution of observed images. These features suggest that observational signatures of chaos in the KSBH spacetime could be explored with future high-resolution observations of BHs environments.
6. Finally, the present analysis can be extended to the study of timelike geodesics and applied to a wider class of BH spacetimes arising in string theory and alternative theories of gravity. Such extensions would allow a more comprehensive understanding of how different geometric structures and additional physical parameters influence nonlinear orbital dynamics and chaotic behavior, thereby offering a broader framework for exploring strong-gravity phenomena beyond the KSBH geometry.

Acknowledgements The authors express sincere gratitude to the anonymous referee for their invaluable feedback and insights, which greatly contributed to the improvement of this manuscript. P.S. acknowledges the University Grants Commission (UGC), New Delhi, India, for financial support as a Junior Research Fellow under UGC Ref. No. 1060/CSIR–UGC NET–June 2018. H.N. acknowledges financial support from the Anusandhan National Research Foundation (ANRF), through the Science and Engineering Research Board (SERB) Core Research Grant (Grant No. CRG/2023/008980).

Data Availability Statement This manuscript has no associated data. [Authors' comment: Data sharing not applicable to this article as no datasets were generated or analysed during the current study.]

Code Availability Statement Code/software will be made available on reasonable request. [Authors' comment: The code/software generated during and/or analysed during the current study is available from the corresponding author on reasonable request.]

Funded by SCOAP[3].

References

1. B. Zwiebach, *A First Course in String Theory* (Cambridge University Press, Cambridge, 2004)
2. D. Lüst, S. Theisen, *Lectures on String Theory*, vol. 346 (Springer, Berlin, 1989)
3. J.B Hartle, Gravity: An Introduction to Einstein's General Relativity (American Association of Physics Teachers, 2003)
4. B. O'Neill, *The Geometry of Kerr Black Holes* (Courier Corporation, North Chelmsford, 2014)
5. S.R. Dolan, Instability of the proca field on kerr spacetime. Phys. Rev. D **98**(10), 104006 (2018)
6. T. Houri, D. Kubizňák, C.M. Warnick, Y. Yasui, Generalized hidden symmetries and the kerr-sen black hole. J. High Energy Phys. **2010**(7), 1–33 (2010)
7. B. Gwak, Cosmic censorship conjecture in kerr-sen black hole. Phys. Rev. D **95**(12), 124050 (2017)
8. S.V.M.C.B. Xavier, P.V.P. Cunha, L.C.B. Crispino, C.A.R. Herdeiro, Shadows of charged rotating black holes: Kerr-newman versus kerr-sen. Int. J. Mod. Phys. D **29**(11), 2041005 (2020)
9. S. Roy, S. Kala, A. Singha, H. Nandan, A.K. Sen, Deflection of light due to Kerr Sen black hole in heterotic string theory using material medium approach. Eur. Phys. J. C **85**(7), 772 (2025)
10. S. Chandrasekhar, S. Chandrasekhar, *The Mathematical Theory of Black Holes*, vol. 69 (Oxford University Press, Oxford, 1998)
11. R. Uniyal, H. Nandan, K.D. Purohit, Null geodesics and observables around the kerr-sen black hole. Class. Quantum Gravity **35**(2), 025003 (2017)
12. D. Garfinkle, G.T. Horowitz, A. Strominger, Erratum: charged black holes in string theory. Phys. Rev. D **45**(10), 3888 (1992)
13. P. Sharma, H. Nandan, G.G.L. Nashed, S. Giri, A. Abebe, Geodesics of a static charged black hole spacetime in f (r) gravity. Symmetry **14**, 309 (2022)
14. A. Simpson, M. Visser, The eye of the storm: a regular kerr black hole. J. Cosmol. Astropart. Phys. **2022**(03), 011 (2022)
15. Y. Lin, Lyapunov function techniques for stabilization. PhD thesis, Rutgers The State University of New Jersey-New Brunswick (1992)
16. S. Sastry, Lyapunov stability theory, in *Nonlinear Systems* (Springer, 1999), pp. 182–234
17. I. Goldhirsch, P.-L. Sulem, S.A. Orszag, Stability and Lyapunov stability of dynamical systems: a differential approach and a numerical method. Phys. D **27**(3), 311–337 (1987)
18. E. Hackmann, Geodesic equations in black hole space-times with cosmological constant. PhD thesis, Universität Bremen (2010)
19. A. Aceña, E. López, F. Aldás, Circular geodesics stability in a static black hole in new massive gravity. Galaxies **8**(1), 14 (2020)
20. H. Abolghasem, Stability of circular orbits in Schwarzschild spacetime. Int. J. Differ. Equ. Appl. **12**(3), 131–147 (2013)

21. V. Cardoso, A.S. Miranda, E. Berti, H. Witek, V.T. Zanchin, Geodesic stability, Lyapunov exponents, and quasinormal modes. Phys. Rev. D **79**(6), 064016 (2009)
22. N.J. Cornish, J. Levin, Lyapunov timescales and black hole binaries. Class. Quantum Gravity **20**(9), 1649 (2003)
23. D. Eberly, *Stability Analysis For Systems Of Differential Equations* (Geometric Tools, LLC, 2008)
24. M. Sandri, Numerical calculation of Lyapunov exponents. Math. J. **6**(3), 78–84 (1996)
25. Yu. Chengye, D. Chen, C. Gao, Bound on Lyapunov exponent in Einstein–Maxwell-dilaton-axion black holes. Chin. Phys. C **46**(12), 125106 (2022)
26. P.P. Pradhan, Lyapunov exponent and charged Myers–Perry spacetimes. Eur. Phys. J. C **73**(6), 2477 (2013)
27. P. Pradhan, Stability analysis and quasinormal modes of Reissner–Nordstrøm space-time via Lyapunov exponent. Pramana **87**(1), 5 (2016)
28. A. Monia, M. Kumar, A.K. Malik, Effect of modulating parameters in chaos and Lyapunov exponent. Math. Stat. Eng. Appl. **71**(3s2), 1213–1223 (2022)
29. S. Giri, H. Nandan, L.K. Joshi, S.D. Maharaj, Stability analysis of circular orbits around a charged btz black hole spacetime in a nonlinear electrodynamics model via Lyapunov exponents. Mod. Phys. Lett. A **36**(31), 2150220 (2021)
30. S. Kala, H. Nandan, P. Sharma, M. Elmardi, Geodesics and bending of light around a BTZ black hole surrounded by quintessential matter. Mod. Phys. Lett. A **36**(31), 2150224 (2021)
31. S. Kala, H. Nandan, P. Sharma, Shadow and weak gravitational lensing of a rotating regular black hole in a non-minimally coupled Einstein–Yang–Mills theory in the presence of plasma. Eur. Phys. J. Plus **137**(4), 457 (2022)
32. P. Singh, H. Nandan, L.K. Joshi, N. Handa, S. Giri, Stability of circular geodesics in equatorial plane of kerr spacetime. Eur. Phys. J. Plus **137**(2), 1–9 (2022)
33. A.M. Lyapunov, The general problem of the stability of motion. Int. J. Control **55**(3), 531–534 (1992)
34. S. Suzuki, K. Maeda, Chaos in Schwarzschild spacetime: the motion of a spinning particle. Phys. Rev. D **55**(8), 4848 (1997)
35. F. Pretorius, D. Khurana, Black hole mergers and unstable circular orbits. Class. Quantum Gravity **24**(12), S83 (2007)
36. M. Mondal, P. Pradhan, F. Rahaman, I. Karar, Geodesic stability and quasi normal modes via Lyapunov exponent for hayward black hole. Mod. Phys. Lett. A **35**(30), 2050249 (2020)
37. S. Kala, H. Nandan, K. Maithani, S. Roy, A. Abebe, Null geodesics, thermodynamics, weak gravitational lensing, and black hole shadow characteristics of a Frolov regular black hole with constraints from EHT observations. Eur. Phys. J. Plus **140**(10), 991 (2025)
38. S. Kala, Propagation of massless particles around a BTZ-ModMax black hole. Int. J. Geom. Methods Mod. Phys. **23**(01), 26501008 (2025)
39. S. Kala, J. Singh, Gravitational lensing and shadow around a non-minimally coupled Horndeski black hole in plasma medium. Eur. Phys. J. C **85**(9), 1047 (2025)
40. S. Giri, H. Nandan, Stability analysis of geodesics and quasinormal modes of a dual stringy black hole via Lyapunov exponents. Gen. Relativ. Gravit. **53**(8), 1–27 (2021)
41. S. Giri, H. Nandan, L.K. Joshi, S.D. Maharaj, Geodesic stability and quasinormal modes of non-commutative Schwarzschild black hole employing Lyapunov exponent. Eur. Phys. J. Plus **137**(2), 1–11 (2022)
42. P. Pradhan, Stability of equatorial circular geodesics for Kerr-Newman spacetime via Lyapunov exponent, in *THE THIRTEENTH MARCEL GROSSMANN MEETING: On Recent Developments in Theoretical and Experimental General Relativity*. Astrophysics and Relativistic Field Theories (World Scientific, Singapore, 2015), pp. 1892–1894
43. L. Caiani, L. Casetti, C. Clementi, M. Pettini, Geometry of dynamics, Lyapunov exponents and phase transitions. Phys. Rev. Lett. **79**, 4361–4364 (1997)
44. L. Barreira, *Lyapunov Exponents*, vol. 1002 (Springer, Berlin, 2017)
45. M. Fouchard, E. Lega, C. Froeschlé, C. Froeschlé, On the relationship between fast lyapunov indicator and periodic orbits for continuous flows, in *Modern Celestial Mechanics: From Theory to Applications: Proceedings of the Third Meeting on Celestical Mechanics—CELMEC III, held in Rome, Italy, 18–22 June, 2001* (Springer, 2002), pp. 205–222
46. P. Cipriani, M.T.D. Bari, Fast instability indicator in few dimensional dynamical systems, in *9th Marcel Grossmann Meeting on Recent Developments in Theoretical and Experimental General Relativity, Gravitation and Relativistic Field Theories (MG 9)* (2000)
47. W. Xin, T. Huang, Computation of Lyapunov exponents in general relativity. Phys. Lett. A **313**, 77–81 (2003)
48. X. Wu, T.Y. Huang, H. Zhang, Lyapunov indices with two nearby trajectories in a curved spacetime. Phys. Rev. D **74**, 083001 (2006)
49. W. Xin et al., Lyapunov indices with two nearby trajectories in a curved spacetime. Phys. Rev. D **74**(8), 083001 (2006)
50. D. Cao, L. Zhang, S. Chen, Q. Pan, J. Jing, Chaotic motion of particles in the spacetime of a Kerr black hole immersed in swirling universes. Eur. Phys. J. C **85**(1), 28 (2025)
51. M. Sano, Y. Sawada, Measurement of the Lyapunov spectrum from a chaotic time series. Phys. Rev. Lett. **55**(10), 1082 (1985)
52. C. Skokos, The Lyapunov characteristic exponents and their computation, in *Dynamics of Small Solar System Bodies and Exoplanets* (Springer, 2010), pp. 63–135
53. H.M. Siahaan, Destroying kerr-sen black holes. Phys. Rev. D **93**(6), 064028 (2016)
54. S.G. Ghosh, R. Kumar, S.U. Islam, Parameters estimation and strong gravitational lensing of nonsingular kerr-sen black holes. J. Cosmol. Astropart. Phys. **2021**(03), 056 (2021)
55. M. Zhang, J. Jiang, Escape probability of particle from kerr-sen black hole. Nucl. Phys. B **964**, 115313 (2021)
56. R.N. Izmailov, R. Kh Karimov, A.A. Potapov, K.K. Nandi, String effect on the relative time delay in the kerr-sen black hole. Ann. Phys. **413**, 168069 (2020)
57. M.F.A.R. Sakti, Hidden conformal symmetry for dyonic kerr-sen black hole and its gauged family. Eur. Phys. J. C **83**(3), 255 (2023)